

Spin Glass Overlap Barriers in Three and Four Dimensions*

Bernd A. Berg

Department of Physics, The Florida State University, Tallahassee, FL 32306, USA.

and

Supercomputer Computations Research Institute,
The Florida State University, Tallahassee, FL 32306, USA.

E-mail: `berg@scri.fsu.edu`

Alain Billoire

CEA/Saclay, Service de Physique Théorique, 91191 Gif-sur-Yvette, France

E-mail: `billoir@spt.saclay.cea.fr`

and

Wolfhard Janke

Institut für Theoretische Physik, Universität Leipzig, 04109 Leipzig, Germany

E-mail: `wolfhard.janke@itp.uni-leipzig.de`

Revised: January 8, 2000

Abstract

For the Edwards-Anderson Ising spin-glass model in three and four dimensions ($3d$ and $4d$) we have performed high statistics Monte Carlo calculations of those free-energy barriers F_B^q which are visible in the probability density $P_{\mathcal{J}}(q)$ of the Parisi overlap parameter q . The calculations rely on the recently introduced multi-overlap algorithm. In both dimensions, within the limits of lattice sizes investigated, these barriers are found to be non-self-averaging and the same is true for the autocorrelation times of our algorithm. Further, we present evidence that barriers hidden in q dominate the canonical autocorrelation times.

PACS. 75.10.Nr Spin-glass and other random models, 75.40.Mg Numerical simulation studies, 75.50.Lk Spin glasses and other random magnets.

*This research was partially funded by the Department of Energy under contracts DE-FG02-97ER41022 and DE-FG05-85ER2500.

1 Introduction

Spin glasses (for reviews see references [1, 2, 3, 4]) constitute an important class of materials whose low-temperature state is a frozen disordered one. In order to produce such a state, there must be randomness and frustration among the different interactions between the spins (magnetic moments). Frustration means that no single spin configuration is favored by all interactions. In real materials such competing interactions are for instance created by magnetic impurity moments. The study of spin glasses developed essentially since the middle of the 1970's and is based on three approaches: experiment, theory and computer simulation.

Experimentally it is not hard to find spin glasses [2]. One kind of widely studied systems consists of dilute solutions of transition metal magnetic impurities in noble hosts. The impurity moments produce a magnetic polarization of the host metal conduction electrons which is positive at some distances and negative at others. Because of the random placements of the impurities they have random, competing interactions with one another. Spin glass states have also been found in magnetic insulators and amorphous alloys. Properties analogous to those of spin glasses, with the electric dipole moment playing the role of the magnetic one, have been seen in ferroelectric-antiferroelectric mixtures. The universal behavior of the observed phenomena is a major reason for the interest in these systems.

A freezing temperature T_c may be defined by a cusp in the ac susceptibility and has, for instance, been studied for Cu-0.9% Mn [5]. Below this transition temperature characteristic non-equilibrium phenomena are observed. A typical experiment is the measurement of the remanent magnetization, see [6] for a study of $(\text{Fe}_{0.15}\text{Ni}_{0.85})_{75}\text{P}_{16}\text{B}_6\text{Al}_3$. A spin-glass sample is rapidly cooled in a magnetic field to a temperature below the transition temperature and the observation is that the decay of the magnetization depends on the waiting time after which the field is switched off. This phenomenon is called aging and has also been found in other disordered or amorphous systems such as structural glasses, polymers, high-temperature superconductors, and charge-density wave systems. These large characteristic time scales suggest the presence of many equilibrium or metastable configurations with a distribution of free-energy barriers separating them.

For free-energy barriers in spin glasses a major complication arises from the fact that there is no parametrization of the relevant configurations by a conventional thermodynamic variable. In his work [7] on the mean-field theory of spin glasses Parisi generalized the

concept of an order parameter. In later language [1, 2, 3, 4] this is expressed as follows: A spin-glass realization is defined by a set of frozen, disordered exchange coupling constants $\mathcal{J} = \{J_{ik}\}$ and for each realization the Parisi overlap parameter is defined by

$$q = \frac{1}{N} \sum_{i=1}^N s_i^1 s_i^2, \quad (1)$$

where the sum goes over the total number N of spins of the system and the spin superscripts label two (real) replica of the same realization. For given \mathcal{J} the probability density of q is denoted by $P_{\mathcal{J}}(q)$ and its cumulative distribution function is $x_{\mathcal{J}}(q) = \int_{-q}^q dq' P_{\mathcal{J}}(q')$. Average over the disorder defines the functions

$$P(q) = [P_{\mathcal{J}}(q)]_{\text{av}} = \frac{1}{\#J} \sum_{\mathcal{J}} P_{\mathcal{J}}(q) \quad \text{and} \quad x(q) = [x_{\mathcal{J}}(q)]_{\text{av}} = \frac{1}{\#J} \sum_{\mathcal{J}} x_{\mathcal{J}}(q),$$

where $\#J$ is the number of realizations considered. In the infinite volume limit below the freezing temperature an increasing *continuous* part of $x(q)$ characterizes mean-field behavior of spin glasses, whereas in ferromagnets as well as in the droplet picture [8] of spin glasses $x(q)$ is a step function.

Analytical calculations in mean-field theory show that violations of the fluctuation-dissipation theorem in non-equilibrium dynamics determine the static function $x(q)$ and vice versa [9], see [10] for a review. Numerical calculations in $3d$ and $4d$ Ising spin glasses [11, 12] support that this relationship holds also in finite dimensions. Of course, the entire $P_{\mathcal{J}}(q)$ set contains more information than its mean $P(q)$ (equivalently $x(q)$). In this paper we study the distribution of the minima in q of the $P_{\mathcal{J}}(q)$ probability densities. For given \mathcal{J} the non-trivial (*i.e.* away from $q = \pm 1$) minima are related to free-energy barriers of the disordered system \mathcal{J} . The other way round, it is presumably model dependent (and worthwhile to investigate) to what extent free-energy barriers of the system \mathcal{J} are reflected in the minima of the $P_{\mathcal{J}}(q)$ probability density.

Conventional, canonical Monte Carlo (MC) simulations do not allow for an efficient investigation of the $P_{\mathcal{J}}(q)$ minima, because the likelihood to generate corresponding configurations in the Gibbs canonical ensemble is small. This problem is overcome by the multi-overlap MC algorithm [13] which samples with an uniform distribution in q . It belongs to the class of multicanonical and related algorithms [14, 15], which allow to focus on rare configurations of the Gibbs ensemble. For instance, at first-order phase transitions in $3d$, configurations with interfaces are suppressed according to $\exp(-\sigma A_{\text{min}})$, where σ is the interface tension and

A_{\min} is the minimal area of the interface. For temperature driven transitions configurations with interfaces are found for E in the energy range $E_1 < E < E_2$ where $E_2 = E_1 + \Delta E$ and ΔE is the latent heat of the transition. To generate such configurations with a good statistics it is sufficient to sample with a weight factor $w(E) \sim 1/n(E)$, where $n(E)$ is the spectral density. Similarly, interfaces for magnetic field driven first-order phase transitions can be generated by sampling with an appropriate weight function $w(M)$ of the magnetization M of the sample.

Once $P_{\mathcal{J}}(q)$ is determined, we define the associated free-energy barrier F_B^q through the autocorrelation time of a $1d$ Markov process which has the canonical $P_{\mathcal{J}}(q)$ distribution as equilibrium state. The barrier autocorrelation time τ_B^q is then defined through the second largest eigenvalue of the transition matrix of this Markov process and the free-energy barrier is $\ln(\tau_B^q)$.

In previous literature [16, 17, 18, 19, 20, 21] investigations of spin-glass barriers relied on various numerical and analytical methods, which are distinct from ours. The results of [16, 17, 18, 19, 20] may be summarized as support of a scaling law $F_B^{\text{can}} \sim N^{1/3}$ for canonical free-energy barriers in the mean-field limit below the freezing temperature.

In the next section we describe our methods and give an overview of our MC statistics. Section 3 presents and interprets our numerical results for free-energy barrier in q . Conclusions and an outlook are given in the final section 4.

2 Overview of Methods and Data

The energy of the Edwards-Anderson Ising (EAI) [22] spin-glass model is given by

$$E = - \sum_{\langle ik \rangle} J_{ik} s_i s_k , \quad (2)$$

where the sum is over nearest-neighbor pairs of a (hyper) cubic lattice. The spins s_i as well as the coupling constants J_{ik} take on the values ± 1 , with equal probabilities, *i.e.* the sum $N^{-1} \sum_{\langle ik \rangle} J_{ik}$ is of order $1/\sqrt{N}$.

In our calculations we combine the two copies (replica) of the same realization and simulate with a weight function

$$w(q) = \exp \left[-\beta(E^1 + E^2) + S(q) \right] . \quad (3)$$

Here $\beta = J_0/k_B T$ is the inverse temperature in natural units, E^1 and E^2 are the energies of the respective replicas and $S(q)$ has the meaning of the microcanonical entropy of the

Parisi order parameter (1). The multi-overlap algorithm weights spin configurations with an overlap parameter q in such a way that a broad histogram in q , eventually covering the entire accessible range $-1 \leq q \leq 1$, is obtained. This allows then for accurate calculations of the empirical probability density $P_{\mathcal{J}}(q)$ of the Parisi order parameter for realization \mathcal{J} . Although an explicit order parameter does not exist, our simulation method [13] is in this way similar to the multimagnetical [15], which for ferromagnetic systems is a very efficient way to sample configurations with interfaces.

Our EAI simulations are performed on $N = L^d$ ($d = 3, 4$) lattices at $\beta = 1$ ($3d$) and $\beta = 0.6$ ($4d$). Both values correspond to temperatures $T = 1/\beta$ below the freezing temperature of the respective model ($\beta_c = 0.90 \pm 0.03$ ($3d$) [23], $\beta_c = 0.485 \pm 0.005$ ($4d$) [24]). Table 1 summarizes the statistics we have assembled as well as the performance of our code. MC updates are given in units of *sweeps*. Our J_{ik} realizations were drawn using the pseudo random number generators RANMAR [25] and RANLUX [26] (luxury level 4). In the simulations themselves we always employed the RANMAR generator due to CPU time considerations.

For each realization \mathcal{J} the simulation consisted of three steps:

1. Construction of the weight function (3). Here we employed an improved variant of the accumulative stochastic iteration scheme discussed in Ref. [27], algorithmic details will be published elsewhere [28]. The iteration was stopped after at least 4 tunneling events

$$(q = 0) \rightarrow (q = \pm 1) \text{ and back} \quad (4)$$

occurred. Our precise request was in $3d$ 10 tunneling events for $L = 4, 6$, and 8, and 20 events for $L = 12$, but for a few cases with only 4 events requested. In $4d$ it was 10 for $L = 4$, 20 for $L = 6$ and 20 to 30 for $L = 8$. In few cases, the system was tunneling so rarely between $q = \pm 1$ that we decided to abort the run and restart with a different random number seed, which in most cases led (eventually after multiple tries) to improved tunneling performance. After the weight function is constructed and kept fixed, the average number of sweeps it takes to create a tunneling event (4) defines the autocorrelation time of the multi-overlap algorithm which in the following is denoted by

$$\tau^{\text{muq}} . \quad (5)$$

Of course, τ^{muq} depends on the realization \mathcal{J} at hand, and on the parameters used in phase 1: random number seed, number of tunneling events requested, etc..

2. Equilibration run. This run of $n \times 65536$ sweeps was done to equilibrate the system for given fixed weight factors ($n = 1, 4, 16, 32$ for $3d$ $L = 4, 6, 8, 12$ and $n = 2, 8, 16$ for $4d$ $L = 4, 6, 8$, respectively).
3. Production run. Each production run of data taking was concluded after at least 20 tunneling events as defined in equation (4) were recorded. To allow for standard reweighting in temperature we stored besides histograms of the Parisi overlap parameter also a time series of measurements for the order parameter, energies and magnetizations of the two replica. The number of sweeps between two successive points in a time series is adjusted in such a way that each time series is made of 65536 measurements. This is done by an adaptive data compression routine [28]. Together with the condition on the minimal number of tunneling events this ensures that the number of sweeps between two successive points in a time series is approximately proportional to τ^{muq} . Some re-weighting results were reported in references [13] and [21], publication of others is intended [28].

With each realization \mathcal{J} we associate the free-energy barrier F_B^q of the $1d$ Metropolis-Markov chain [29] which has the canonical $P_{\mathcal{J}}(q)$ probability density as its equilibrium distribution. The transition probabilities $T_{i,j}$ are given by

$$T = \begin{bmatrix} 1 - w_{2,1} & w_{1,2} & 0 & \dots \\ w_{2,1} & 1 - w_{1,2} - w_{3,2} & w_{2,3} & \dots \\ 0 & w_{3,2} & 1 - w_{2,3} - w_{4,3} & \dots \\ 0 & 0 & w_{4,3} & \dots \\ \vdots & \vdots & \vdots & \ddots \end{bmatrix}, \quad (6)$$

where $w_{i,j}$ ($i \neq j$) is a probability à la Metropolis to jump from state $q = q_j$ to $q = q_i$ ($q_i = i/N$, $i \in [-N, -N + 2, \dots, +N]$),

$$w_{i,j} = \frac{1}{2} \min\left(1, \frac{P_{\mathcal{J}}(q_i)}{P_{\mathcal{J}}(q_j)}\right). \quad (7)$$

T fulfills the detailed balance condition (with $P_{\mathcal{J}}$) and as a consequence it has only real eigenvalues. The largest eigenvalue (equal to one) is non-degenerate, and the second largest eigenvalue λ_1 determines the autocorrelation time of the chain,

$$\tau_B^q = \frac{1}{N(1 - \lambda_1)}, \quad (8)$$

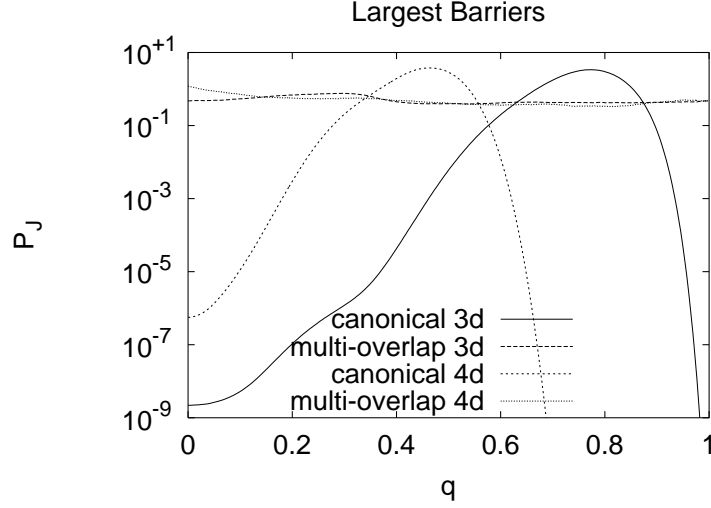


Figure 1: Canonical $P_{\mathcal{J}}(q)$ and (flat) multi-overlap $P_{\mathcal{J}}^{\text{muq}}(q)$ probability densities for our realization with the largest free-energy barrier in $3d$ ($L = 8$) and $4d$ ($L = 8$).

and we define the associated free-energy barrier for realization \mathcal{J} as

$$F_B^q = \ln(\tau_B^q) . \quad (9)$$

For the simple double-peak situation of first-order phase transitions the autocorrelation time τ_B^q is proportional to the ratio $P_{\mathcal{J}}^{\text{max}}/P_{\mathcal{J}}^{\text{min}}$ where

$$P_{\mathcal{J}}^{\text{max}} = P_{\mathcal{J}}(q_{\text{max}}) = \max_q [P_{\mathcal{J}}(q)] \quad \text{and} \quad P_{\mathcal{J}}^{\text{min}} = \min_{0 < q < |q_{\text{max}}|} [P_{\mathcal{J}}(q)] ,$$

i.e. $F_B^q = \ln[P_{\mathcal{J}}^{\text{max}}/P_{\mathcal{J}}^{\text{min}}] + \text{const.}$ This leads in $3d$ to $\tau_B^q \sim e^{\sigma A_{\text{min}}}$ and $F_B^q \sim \sigma A_{\text{min}} + \text{const.}$, where A_{min} is the minimal area between the coexisting phase regions and σ is the interfacial tension. Equation (9) is the appropriate generalization to a situation involving multiple minima and maxima. The autocorrelation time τ_B^q has to be regarded as a lower limit to the canonical autocorrelation time τ^{can} for the Markov process where the spin variables are the dynamical degrees of freedom. The definition (8) takes only barriers in q into account but not other barriers which may well exist in the multi-dimensional configuration space.

The matrix T in (6) is tri-diagonal and sign symmetric. This special form allows for easy calculation of all its eigenvalues [30]. The realizations with the largest thus obtained free-energy barriers in $3d$ and $4d$ are depicted in figure 1. Both do not show a complicated landscape, but a plain two-peak structure. Besides the canonical $P_{\mathcal{J}}(q)$ probability densities the essentially flat probability densities $P_{\mathcal{J}}^{\text{muq}}(q)$ of the multi-overlap simulation are also

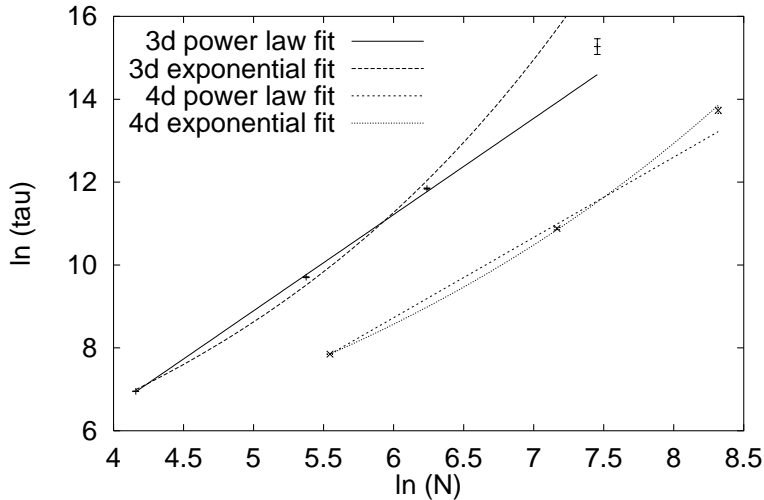


Figure 2: Power law and exponential fits for the mean multi-overlap tunneling time $[\tau^{\text{muq}}]_{\text{av}}$ in $3d$ and $4d$.

indicated in the figure. Both $P_{\mathcal{J}}(q)$ probability densities take their minimum at $q = 0$ and we have $P_{\mathcal{J}}^{\text{max}}/P_{\mathcal{J}}^{\text{min}} > 10^8$ in $3d$ ($L = 8$) and $P_{\mathcal{J}}^{\text{max}}/P_{\mathcal{J}}^{\text{min}} > 10^6$ in $4d$ ($L = 8$); compare also table 2. The improvement factors in computer time are directly proportional and close to these numbers which reflect the enhancements in visits of $P_{\mathcal{J}}(0)$ as compared to canonical simulations. Multiplying the improvement factors with the average CPU times needed by the multi-overlap algorithm for a single realization on lattices of this size (see table 1), it becomes clear that exploration of such barriers by means of a canonical MC simulation is simply impossible.

We conclude this section with remarks about the performance of the algorithm and implications on the physics of the system. The multi-overlap algorithm flattens the free-energy barriers F_B^q . If they were the only cause for the slowing down of the canonical dynamics, the multi-overlap autocorrelation time should be dominated by a random walk behavior between $q = -1$ and $q = +1$ and scale proportional to N (in units of sweeps). Fitting the estimates of the mean autocorrelation time $[\tau^{\text{muq}}]_{\text{av}}$, where the average is with respect to the realizations \mathcal{J} , to the power-law form $\ln([\tau^{\text{muq}}]_{\text{av}}) = a + z \ln(N)$ gives $z = 2.32 \pm 0.07$ in $3d$ and $z = 1.94 \pm 0.02$ in $4d$. The fits are depicted in figure 2. Their quality is bad, nevertheless they show that the slowing down is quite off from the theoretical optimum $z = 1$. Exponential fits $\ln([\tau^{\text{muq}}]_{\text{av}}) = c_0 + c_1 N$ are also depicted in the figure.

Whereas in $3d$ the exponential fit is far worse than the power-law fit, it is the other way round in $4d$. Hence, the smaller z -value in $4d$ should not be taken seriously.

The physically important conclusion is: the observed large autocorrelation times demonstrate that, in the model considered, canonical overlap barriers are not an exclusive cause for the slowing down of spin-glass dynamics below the freezing temperature. Therefore, τ_B^q has to be a lower bound of the full canonical autocorrelation time τ^{can} :

$$\tau_B^q < \tau^{\text{can}} . \quad (10)$$

One should understand q as one relevant direction in a complex, multidimensional configuration space. By depicting free-energy barriers as function of q one projects on this direction and averages results over all other directions.

3 Barrier Results

We analyze our free-energy barrier densities relying on a variant of the cumulative distribution function F . For a set of sorted data

$$x_1 < x_2 < \dots < x_n \quad (11)$$

the (empirical) cumulative distribution function $F(x)$, see for instance [31], is defined by

$$\frac{i}{n} - \frac{1}{2n} \leq F(x) \leq \frac{i}{n} + \frac{1}{2n} \quad \text{for } x_i \leq x \leq x_{i+1} , \quad (12)$$

where we use a straight-line interpolation in-between. Next we define a Q -tile [32] distribution function as introduced in [33]

$$F_Q(x) = \begin{cases} F(x) & \text{for } F(x) \leq 0.5 ; \\ 1 - F(x) & \text{for } F(x) \geq 0.5 . \end{cases} \quad (13)$$

This function peaks at the median x_{med} of the data and takes there the value $F_Q = 0.5$. For self-averaging data x the function F_Q collapses in the infinite volume to

$$F_Q(x) = \begin{cases} 0.5 & \text{for } x = \bar{x} ; \\ 0 & \text{otherwise .} \end{cases}$$

Here \bar{x} is the mean value. For non-averaging quantities the width of F_Q stays finite. The concept carries over to observables which diverge in the infinite volume limit, when on each lattice size results are expressed in units of the respective median value, *i.e.* instead of an observable X the ratio $x = X/X_{\text{med}}$ is used.

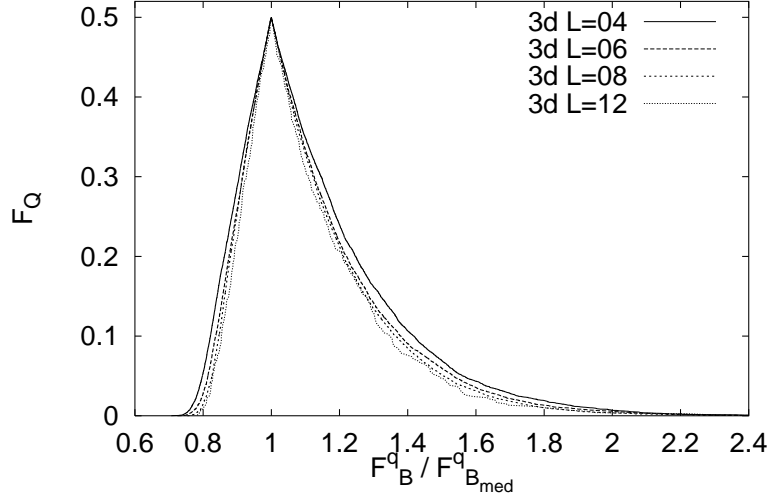


Figure 3: Distribution function F_Q (13) for the $3d$ overlap barriers (9) in units of their median value.

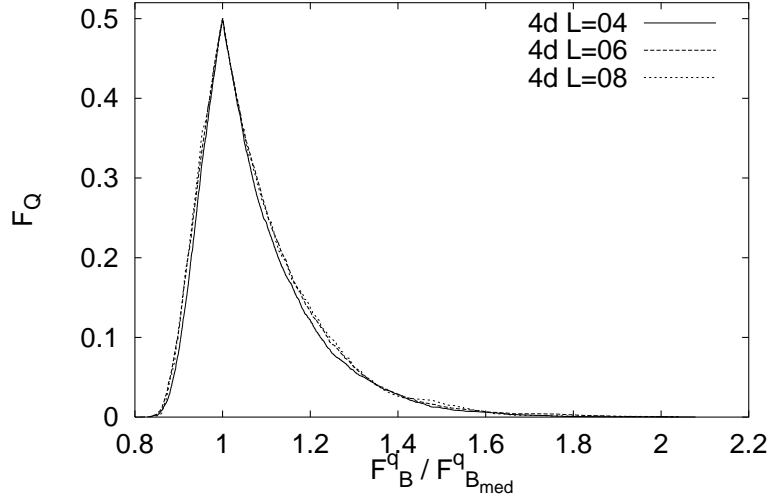


Figure 4: Distribution function F_Q (13) for the $4d$ overlap barriers (9) in units of their median value.

3.1 Lack of self-averaging

For the free-energy barriers (9) we have depicted our thus obtained $F_Q(F_B^q/F_{B,med}^q)$ functions in figures 3 ($3d$) and 4 ($4d$). For each lattice the measured F_B^q values were first sorted as function of \mathcal{J} such that

$$F_{B,1}^q < F_{B,2}^q < \dots < F_{B,n}^q ,$$

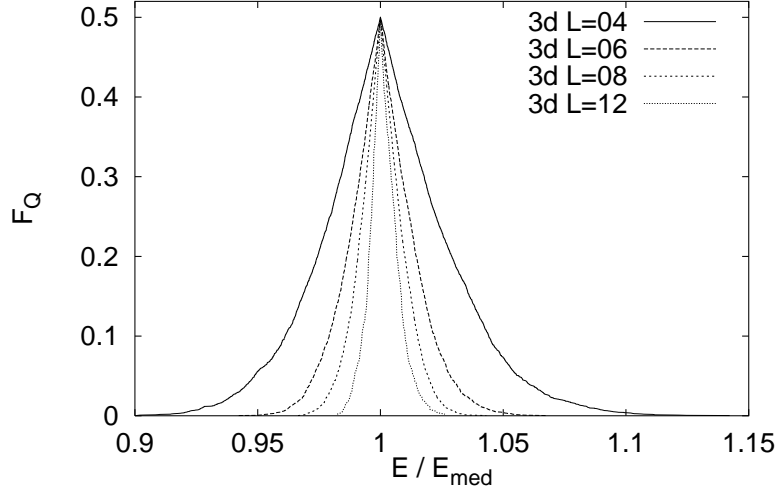


Figure 5: Distribution function F_Q (13) for the $3d$ energies (2) in units of their median value.

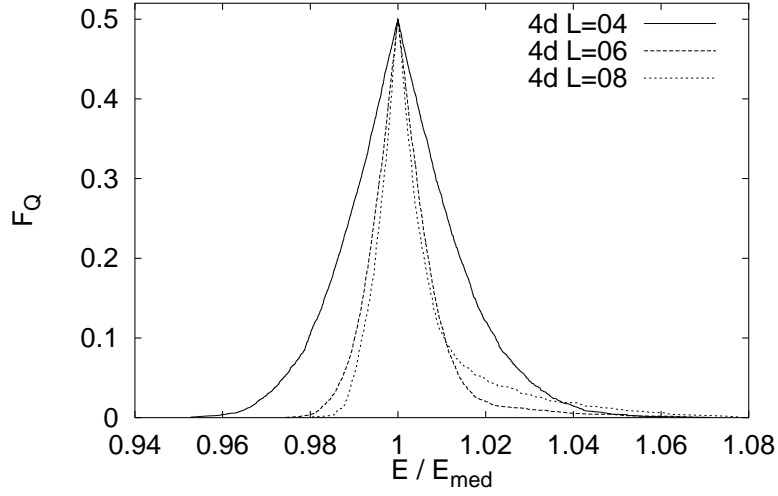


Figure 6: Distribution function F_Q (13) for the $4d$ energies (2) in units of their median value.

where n is the number of realizations $\#\mathcal{J}$ given in table 1. Subsequently $F_{B,\text{med}}^q$ was calculated as

$$F_{B,\text{med}}^q = \frac{1}{2} \left(F_{B,n/2}^q + F_{B,1+n/2}^q \right) \quad (n \text{ is even in our cases}),$$

and F_Q computed for $x = F_B^q / F_{B,\text{med}}^q$.

Both figures support that F_B^q is a non-self-averaging quantity. This is stronger in $4d$ than in $3d$, because the inner lines belong in $3d$ to the larger lattices, whereas in $4d$ it is the other

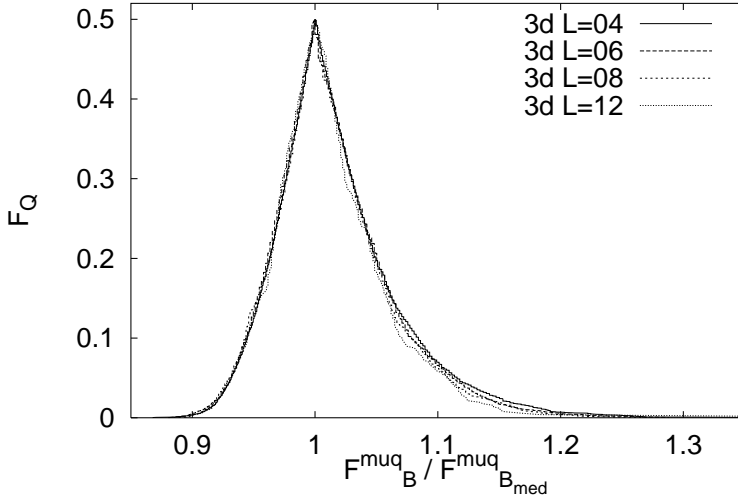


Figure 7: Distribution function F_Q (13) for the $3d$ barriers (14) of the multi-overlap algorithm in units of their median value.

way round. However, in both cases there are marginal finite-size effects, whereas finite-size dependence of self-averaging is expected to be rather strong. This becomes obvious when comparing with an observable which is supposed to be self-averaging. Namely, figures 5 ($3d$) and 6 ($4d$) depict the same analysis for the internal energy (2). In $3d$ self-averaging of this quantity is obvious, whereas in $4d$ there is an irregularity when going from $L = 6$ to $L = 8$. As our simulation temperature in $4d$ is quite low, we think that this behavior is related to groundstate irregularities on small lattices (only the corresponding half of the distribution is affected). For both $3d$ and $4d$ the q -tile distribution function of the energy is strongly peaked around $E/E_{\text{med}} = 1$, whereas the overlap barrier distributions are much broader.

It is generally believed that, in contrast to the equilibrium autocorrelation times considered here, non-equilibrium autocorrelations are self-averaging [10]. No sample-to-sample deviations have been reported for real experiments [6] and self-averaging is also used for measurements of non-equilibrium properties in MC simulations [11, 12].

The multi-overlap algorithm eliminates the free-energy barriers which are visible in the $P_{\mathcal{J}}(q)$ probability densities. Let us therefore focus on the autocorrelations times of this algorithm and its barriers defined by

$$F_B^{\text{muq}} = \ln(\tau^{\text{muq}}) . \quad (14)$$

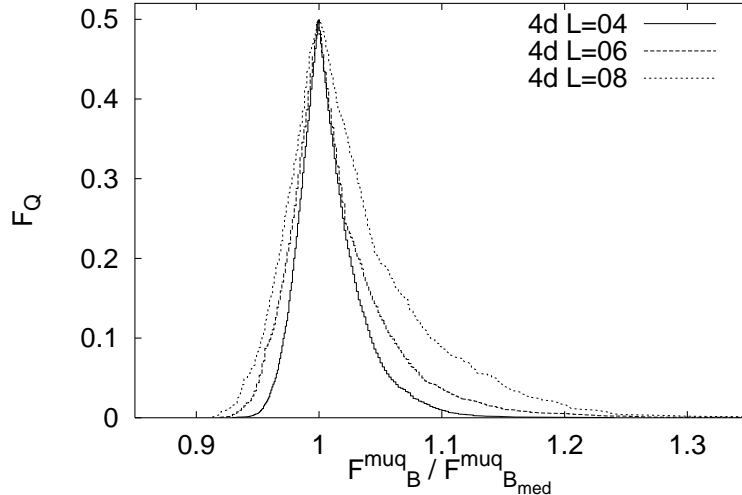


Figure 8: Distribution function F_Q (13) for the $4d$ barriers (14) of the multi-overlap algorithm in units of their median value.

We perform the analysis along our previous lines and show in figures 7 (3d) and 8 (4d) the thus obtained $F_Q(F_B^{\text{muq}}/F_{B,\text{med}}^{\text{muq}})$ functions. Lack of self-averaging is even more obvious than for F_B^q . In figure 7 (3d) there are (within the statistical accuracy) no finite-size effects visible and figure 8 (4d) exhibits a strong anti-self-averaging trend: Results for the larger lattices move to the outside instead to the inside.

3.2 Finite-size scaling behavior

In this final part of section 3 we discuss how data (experimental or MC) for non-self-averaging observables may be analyzed such that comparisons of results from different groups become possible. One has to investigate many samples and should report the finite-size scaling behavior for fixed values of the cumulative distribution function F (12). In particular this includes $F = 1/2$ which defines the median value. We exemplify this for the overlap autocorrelation time τ_B^q (8), but the method applies for non-self-averaging observables in general.

From figures 3 and 4 it is obvious that the autocorrelation times τ_B^q will have long tails towards large values. This implies that the mean value over all samples is a rather erratic quantity which is dominated by a few rare realizations. Table 2 collects the mean, median ($F = 1/2$) and maximum ($F = 1 - 1/(2n)$) values for τ_B^q . The numbers in parenthesis indicate error bars in the last digits of the quantity given before. The results show that contributions

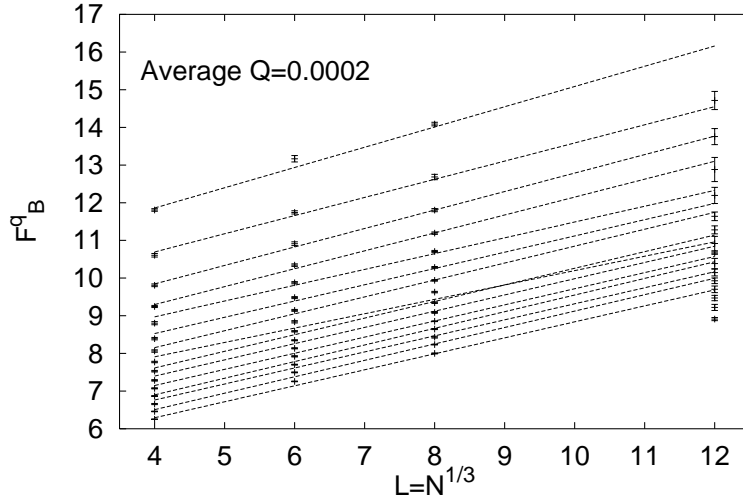


Figure 9: Fits (15) of the 3d free-energy barriers F_B^q versus $N^{1/3}$ corresponding to the exponential finite-size scaling behavior (16) of τ_B^q . From down to up the lines are at $16 F = 1, 3, 5, 7, 9, 11, 12, 13, 14,$ and 15 .

of the maximum values dominate to a large extent the mean values (just divide the maximum values by the number of realizations and compare the results with the mean values). The maximum values rely on realizations \mathcal{J} of likelihood $1/n$, what explains their very large errors. In contrast to the mean and the maximum, results for fixed F remain well defined as long as F stays away from its extreme values $1/n$ and $1 - 1/n$. In particular, note that samples with relaxation times too long to be measured can still contribute to determine the correct F values for smaller relaxation times.

In the following we focus on our results for the free-energy barriers F_B^q at $F = i/16$ with $i = 1, \dots, 15$. For each F value we performed fits to the form

$$F_B^q = a_1 + a_2 N^{1/3} \quad (15)$$

which corresponds to the exponential finite-size scaling behavior

$$\tau_B^q = e^{a_1} e^{a_2 N^{1/3}} \quad (16)$$

suggested by investigations of autocorrelation times and barriers in the mean-field limit [16, 17, 18, 19, 20]. These fits are depicted in figures 9 and 10. Examples of the fit parameters a_1 and a_2 are collected in table 3; for all fits given there, the goodness-of-fit parameter Q [31] is smaller than 0.003. The average Q over all 15 fits is given in the figures. For consistent

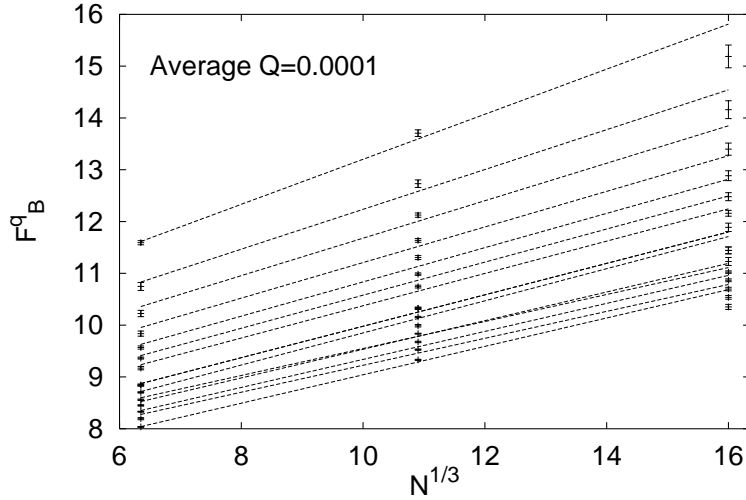


Figure 10: Fits (15) of the 4d free-energy barriers F_B^q versus $N^{1/3}$ corresponding to the exponential finite-size scaling behavior (16) of τ_B^q . From down to up the lines are at 16 $F = 1, 3, 5, 7, 9, 11, 12, 13, 14,$ and 15.

fits the expectation for the Q -average is 1/2 and the quality of our 3d and 4d exponential fits is unacceptable. We therefore try a power-law fit

$$\tau_B^q = c N^\alpha , \quad (17)$$

which corresponds to a fit of the form

$$F_B^q = \ln(c) + \alpha \ln(N) . \quad (18)$$

These fits are depicted in figures 11 and 12. In 3d as well as in 4d the average Q -value is now almost perfect. Examples of the power-law fit parameters and Q -values are given in table 4. They indicate that the distribution of Q -values is less perfect than their mean. Such uncertainties are an intrinsic limitation of MC simulations and become particularly severe when one is, as in our investigation, limited to rather small-sized systems. Having these limitations in mind, the over-all quality of the power-law fits is remarkably good. Our data favor them strongly over the exponential behavior.

As function of F the exponent $\alpha = \alpha(F)$ varies smoothly and covers in 4d a range from 0.8 at $F = 1/15$ to 1.3 at $F = 15/16$. In 3d the range is somewhat smaller, see table 4. Fits for $F > 15/16$ become erratic and it makes little sense to report them. A similar analysis for the autocorrelation times of the multi-overlap algorithm gives exponents $\alpha(F)$ which are

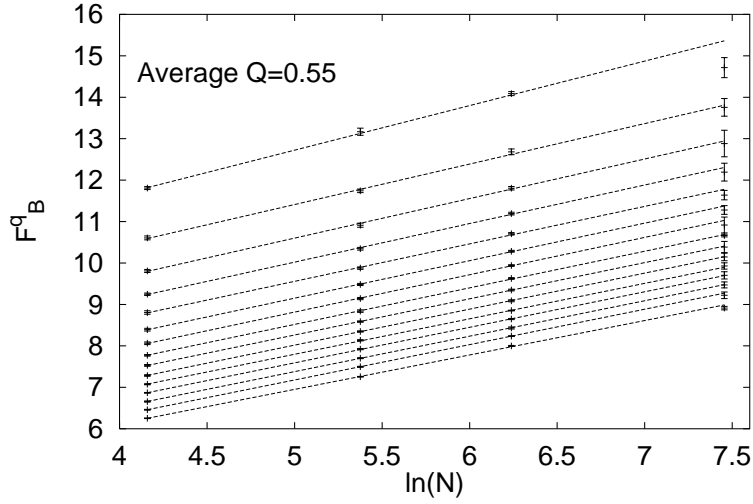


Figure 11: Fits (18) of the 3d free-energy barriers F_B^q versus $\ln(N)$ corresponding to the power-law finite-size scaling behavior (17) of τ_B^q . From down to up the lines are at 16 $F = 1, 3, 5, 7, 9, 11, 12, 13, 14,$ and 15.

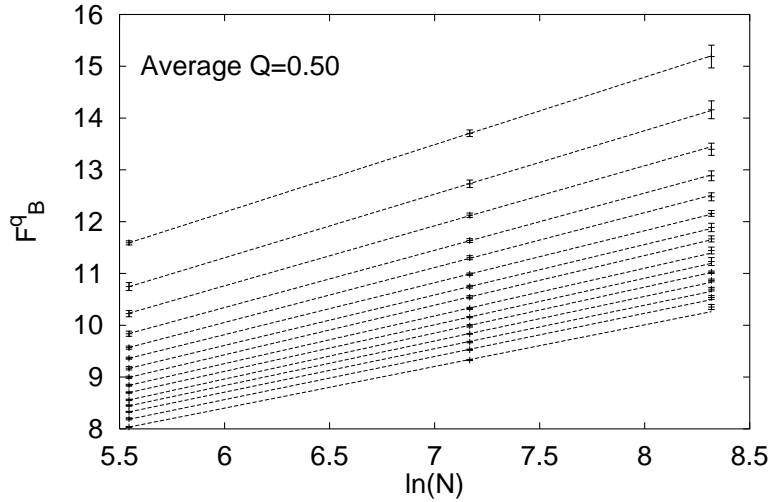


Figure 12: Fits (18) of the 4d free-energy barriers F_B^q versus $\ln(N)$ corresponding to the power-law finite-size scaling behavior (17) of τ_B^q . From down to up the lines are at 16 $F = 1, 3, 5, 7, 9, 11, 12, 13, 14,$ and 15.

larger,

$$\alpha^{\text{muq}}(F) \approx \alpha_B^q(F) + 1 .$$

This re-iterates and sharpens our previous observation that relevant barriers exist, which are invisible in the overlap variable q .

4 Summary and Conclusions

We have investigated free-energy barriers in the Parisi order parameter (1). The results are sample dependent and non-self-averaging on the (admittedly rather small) simulated systems. The power-law behavior (17) of the Markov autocorrelation times τ_B^q as defined in eq. (8) is favored over the exponential behavior (16). To the extent that this behavior extrapolates to the infinite volume limit and that our methods relate to those of Ref. [16, 17, 18, 19, 20], it means that both $3d$ and $4d$ are quite far away from the $d \rightarrow \infty$ mean-field theory limit. As relevant barriers are still found in the autocorrelations of the multi-overlap algorithm, such a relation is far from clear.

Acknowledgements

B.B. likes to thank Wolfgang Grill for his hospitality during an extended stay at Leipzig University in the framework of the *International Physics Studies Program*. Most numerical simulations were performed on the T3E computer of CEA in Grenoble under grant p526, additional calculations were done on T3E computers of ZIB in Berlin under grant bvpl01, and of NIC in Jülich under grant hmz091, and on Alpha workstations at FSU. We thank all institutions for their generous support.

References

- [1] A.P. Young (ed.), *Spin Glasses and Random Fields*, World Scientific, Singapore, 1997.
- [2] K.H. Fischer and J.A. Hertz, *Spin Glasses*, Cambridge University Press, 1991.
- [3] M. Mézard, G. Parisi, and M.A. Virasoro, *Spin Glass Theory and Beyond*, World Scientific, Singapore, 1987.
- [4] K. Binder and A.P. Young, *Spin Glasses: Experimental Facts, Theoretical Concepts and Open Questions*, Rev. Mod. Phys. **56**, 801 (1986).
- [5] C.A.M. Mulder, A.J. van Duynveldt, and J.A. Mydosh, Phys. Rev. **B23**, 1384 (1981); Phys. Rev. **B25**, 515 (1982).
- [6] P. Granberg, P. Svedlindh, P. Nordblad, L. Lundgren, and H.S. Chen, Phys. Rev. **B35**, 2075 (1987); E. Vincent, J. Hammann, M. Ocio, J.-P. Bouchaud, and L.F.

Cugliandolo, in *Complex Behaviour of Glassy Systems*, ed. M. Rubi, Lecture Notes in Physics Vol. 492, Springer Verlag, 1997, pp. 184-219 [cond-mat/9607224], and references given therein.

- [7] G. Parisi, Phys. Rev. Lett. **43**, 1754 (1979).
- [8] D.S. Fisher and D.A. Huse, Phys. Rev. **B38**, 386 (1988).
- [9] L.F. Cugliandolo and J. Kurchan, Phys. Rev. Lett. **71**, 173 (1993); J. Phys. **A27**, 5749 (1994).
- [10] J.-P. Bouchaud, L.F. Cugliandolo, J. Kurchan, and M. Mézard, in Ref. [1], p. 161 ff., section 3.1.
- [11] S. Franz and H. Rieger, J. Stat. Phys. **79**, 749 (1995).
- [12] E. Marinari, G. Parisi, F. Ricci-Tersenghi, and J.J. Ruiz-Lorenzo, J. Phys. **A31**, 2611 (1998).
- [13] B.A. Berg and W. Janke, Phys. Rev. Lett. **80**, 4771 (1998).
- [14] G.M. Torrie and J.P. Valleau, J. Comp. Phys. **23**, 187 (1977); B.A. Berg and T. Neuhaus, Phys. Rev. Lett. **68**, 9 (1992); B.A. Berg and T. Celik, Phys. Rev. Lett. **69**, 2292 (1992); W. Janke and S. Kappler, Phys. Rev. Lett. **74**, 212 (1995); B. Hesselbo and R. Stinchcombe, Phys. Rev. Lett. **74**, 2151 (1995).
- [15] B.A. Berg, U. Hansmann, and T. Neuhaus, Phys. Rev. **B47**, 497 (1993); Z. Phys. **90**, 229 (1993).
- [16] N.D. Mackenzie and A.P. Young, Phys. Rev. Lett. **42**, 301 (1982); J. Phys. **C16**, 5321 (1983).
- [17] K. Nemoto, J. Phys. **A21**, L287 (1988).
- [18] G.J. Rodgers and M.A. Moore, J. Phys. **A22**, 1085 (1989).
- [19] D. Vertechi and M.A. Virasoro, J. Phys. France **50**, 2325 (1989).
- [20] R.N. Bhatt, S.G.W. Colborne, M.A. Moore, and A.P. Young, unpublished, see [18].

- [21] W. Janke, B.A. Berg, and A. Billoire, *Ann. Phys. (Leipzig)* **7**, 544 (1998).
- [22] S.F. Edwards and P.W. Anderson, *J. Phys.* **F5**, 965 (1975).
- [23] N. Kawashima and A.P. Young, *Phys. Rev.* **B53**, R484 (1996).
- [24] D. Badoni, J. C. Ciria, G. Parisi, F. Ritort, J. Pech, and J.J. Ruiz-Lorenzo, *Europhys. Lett.* **21**, 495 (1993).
- [25] G. Marsaglia, A. Zaman, and W.W. Tsang, *Stat. and Prob. Lett.* **8**, 35 (1990).
- [26] M.L. Lüscher, *Comp. Phys. Commun.* **79**, 100 (1994).
- [27] B.A. Berg, *J. Stat. Phys.* **82**, 323 (1996).
- [28] B.A. Berg, A. Billoire, and W. Janke, in preparation.
- [29] N. Metropolis, A.W. Rosenbluth, M.N. Rosenbluth, A.H. Teller, and E. Teller, *J. Chem. Phys.* **21**, 1087 (1953).
- [30] We used the EISPACK subroutines `figi` and `imtq11` which are available on the web at Bell Labs: <http://netlib.bell-labs.com/netlib/eispack/index.html>.
- [31] W.H. Press, B.P. Flannery, S.A. Teukolsky, and W.T. Vetterling, *Numerical Recipes*, Cambridge University Press, 1986.
- [32] Q refers to statistical Q -tiles and q to the Parisi overlap parameter.
- [33] B.A. Berg, *Introduction to Monte Carlo Simulations and Their Statistical Analysis*, in preparation.

Tables

Table 1: *Statistics: Number of realizations $\#\mathcal{J}$, average number of mega-sweeps per realization n_{sw} and average single 375 MHz processor CPU time per realization in hours (h) or seconds (s) as benchmarked on the CEA T3E.*

	3d			4d		
L	$\#\mathcal{J}$	n_{sw}	CPU	$\#\mathcal{J}$	n_{sw}	CPU
4	8 192	0.2 M	6.32 s	4 096	0.4 M	76.6 s
6	8 192	1.0 M	113 s	4 096	3.7 M	1.02 h
8	8 192	7.6 M	0.54 h	1 024	49.3 M	42.66 h
12	640	154.0 M	36.97 h			

Table 2: *Mean, median and maximum values for the Markov autocorrelations times τ_B^q (8).*

L	4	6	8	12
3d: Mean	$61(29) \times 10^4$	$10(06) \times 10^6$	$56(45) \times 10^6$	$13(10) \times 10^7$
3d: Median	$237(05) \times 10^1$	$690(02) \times 10^1$	$152(04) \times 10^2$	$444(05) \times 10^2$
3d: Maximum	$22(20) \times 10^8$	$32(06) \times 10^9$	$35(33) \times 10^{10}$	$53(30) \times 10^9$
4d: Mean	$94(34) \times 10^3$	$23(08) \times 10^5$	$26(23) \times 10^6$	
4d: Median	$807(18) \times 10^1$	$379(11) \times 10^2$	$117(07) \times 10^3$	
4d: Maximum	$13(11) \times 10^7$	$21(07) \times 10^8$	$22(21) \times 10^9$	

Table 3: *Fit parameters for the free-energy barriers fits (15); $Q < 0.003$ for all cases.*

	3d		4d	
F	a_1	a_2	a_1	a_2
1/16	4.59(2)	0.424(03)	6.30(02)	0.274(03)
4/16	5.13(3)	0.442(04)	6.77(03)	0.276(03)
8/16	6.38(4)	0.382(05)	7.13(05)	0.301(06)
12/16	7.39(6)	0.476(11)	7.77(11)	0.344(10)
15/16	9.71(9)	0.538(14)	8.85(12)	0.435(15)

Table 4: *Free energy barriers fits (18): Fit parameters and goodness of fit.*

	3d			4d		
F	$\ln(c)$	α	Q	$\ln(c)$	α	Q
1/16	2.80(03)	0.830(06)	0.04	3.58(05)	0.804(08)	0.05
4/16	3.30(04)	0.857(08)	0.77	3.68(06)	0.860(08)	0.13
8/16	4.10(06)	0.883(10)	0.52	3.68(11)	0.958(18)	0.71
12/16	5.37(11)	0.930(20)	0.51	3.71(22)	1.105(32)	0.81
15/16	7.35(14)	1.075(28)	0.02	4.37(26)	1.302(42)	0.94